

# Antiferromagnetic fluctuations and a dominant $d_{xy}$ -wave pairing symmetry in nickelate-based superconductors

Chao Chen,<sup>1</sup> Runyu Ma,<sup>1</sup> XueLei Sui,<sup>2</sup> Ying Liang,<sup>1</sup> Bing Huang,<sup>2,1</sup> and Tianxing Ma<sup>1,2,\*</sup>

<sup>1</sup>Department of Physics, Beijing Normal University, Beijing 100875, China

<sup>2</sup>Beijing Computational Science Research Center, Beijing 100084, China

Motivated by recent experimental studies on superconductivity found in nickelate-based materials, we study the temperature dependence of the spin correlation and the superconducting pairing interaction within an effective two-band Hubbard model by the quantum Monte Carlo method. Based on parameters extracted from the first principles calculations, our intensive numerical results reveal that the pairing with a  $d_{xy}$ -wave symmetry firmly dominates over other pairings at low temperature, which are mainly determined by the Ni3d orbital. It is also found that the effective pairing interaction is enhanced as the on-site Coulomb interaction increases, demonstrating that the superconductivity is driven by strong electron-electron correlation. Even the  $(\pi, \pi)$  antiferromagnetic correlation could be enhanced by electronic interaction, there are no evidence for the long-range antiferromagnetic order exhibit in nickelate-based superconductors.

*Introduction* Understanding the mechanism of high-Tc superconductivity has always been a central issue in condensed matter physics[1–7]. Recently, the discovery of superconductivity in the family of Sr-doped RNiO<sub>2</sub> (R=Nd, La) has attracted great research interest, which may provide a new opportunity for further understanding unconventional superconductivity[8–24]. Among them, one essential object is to identify the dominant superconducting pairing form, which remains a major challenge of today’s studies on this family. In a single particle tunnelling experiment on a Sr-doped NdNiO<sub>2</sub> film surface, researchers detected singlet pairing, but they could not distinguish whether it was a  $s$ -wave,  $d$ -wave or their mixture[25]. At present, some theoretical studies of nickelate-based superconductors have been based on models with one-orbital (Ni 3d) band structures that support these materials being captured by a one-band Hubbard model[26, 27], and they have obtained a dominant  $d$ -wave pairing in their model[26, 27]. However, others have proposed various possibilities for multiband models[28–32]. The  $t - J - K$  model, which considers the Kondo coupling, exhibits a transition between the  $d$ -wave and  $(d + is)$ -wave of the dominant pairing at large hole doping[33]. Research on the controversial pair symmetry of nickelates is necessary both experimentally and theoretically. From the theoretical viewpoint, using unbiased numerical techniques is believed to be the only opportunity to achieve this goal if the electronic correlation dominates in the system.

Previous theoretical works on density-functional theory (DFT)[10, 34–37] have studied the characteristics of nickelate electronic structures. It was found that there were both similarities and differences compared with those of cuprates[10, 29, 31, 36–40]. These results provide a good background to study the magnetism and superconductivity in the nickelate family. According to the DFT calculation of RNiO<sub>2</sub>[10, 36, 37], the two bands near  $E_F$  mainly contributed to its physical properties. One band, composed of Ni 3d <sub>$x^2-y^2$</sub>  and O 2p

orbitals, has a Zhang-Rice-singlet-like character, while the contribution of oxygen in the nickelate is smaller than that in cuprates, and the other band, composed of R5d orbitals, forms an important metallic electron pocket. These two orbitals hybridize, forming a system, where the strongly correlated Ni layers play an important role[10, 36, 37].

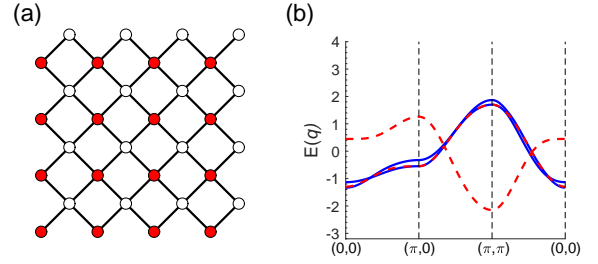


FIG. 1. (Color online)(a) Here, red and white circles indicate different sublattices, A and B. (b) The energy band along the high symmetry line in the unfolded Brillouin zone. Solid blue lines:  $k_z=0$ ; dashed red lines:  $k_z = \pi$  in Table I.

To identify the superconducting pairing form of nickelate-based materials, we perform a quantum Monte Carlo study of the spin correlation and superconducting pairing interaction in an effective two-band microscopic model based on parameters extracted from the first principles calculations. From the results of the Wannier orbitals[10, 36], a two-band model is constructed that contains two main bands near  $E_F$ , and this model also contains inter-orbital coupling between the Ni3d orbital and the R5d orbital. The calculations of the pairing correlation show that there exists an extensive  $d$ -wave channel that firmly dominates over other pairings at low temperature and the pairing channel are determined by the Ni3d orbital. For different fillings ( $n$ )=1.0, 0.9, and 0.8, the  $(\pi, \pi)$  antiferromagnetic (AFM) correlation and the effective pairing interaction are both enhanced as

Hopping parameters for the tight binding model			
$k_z$	0	$\pi/2$	$\pi$
$t$			
		$t^{Nd}$	
$\Delta_1$	0.633	1.305	1.977
$t_1$	-0.380	-0.028	0.324
$t_2$	0.084	-0.090	-0.264
$t_3$	0.003	0.027	0.051
		$t^{Ni}$	
$\Delta_2$	0.242	0.308	0.374
$t_1$	-0.374	-0.374	-0.374
$t_2$	0.094	0.094	0.094
$t_3$	-0.043	-0.043	-0.043
		$t^{Nd-Ni}$	
$t_3$	0.002	0.002	0.002

TABLE I. Hopping parameters for the tight binding model from Refs.[10, 36, 37].

the on-site Coulomb interaction increases. Our unbiased calculations demonstrate that the superconductivity and AFM correlation in nickelate-based superconductors should be driven by electron-electron correlation. Even the  $(\pi, \pi)$  antiferromagnetic correlation could be enhanced by electronic interaction, there are no evidence for the long-range antiferromagnetic order exhibit in nickelate-based superconductors.

*Model and methods* In the extended two-band Hubbard model, the tight-binding part contains intralayer hoppings, interlayer hoppings and the strongly correlated Ni layer. Therefore, the nickel-square lattice Hamiltonian can be written as

$$\begin{aligned}
H &= H_1 + H_2 + H_3 + H_4, \\
H_1 &= t_3^{Nd-Ni} \sum_{i\eta\sigma} [a_{i\sigma}^\dagger b_{i+\eta\sigma} + h.c.], \\
H_2 &= t_1^{Nd} [\sum_{i\tau_1\sigma} a_{i\sigma}^\dagger a_{i+\tau_1\sigma}] + t_2^{Nd} [\sum_{i\tau_2\sigma} a_{i\sigma}^\dagger a_{i+\tau_2\sigma}] \\
&\quad + t_3^{Nd} [\sum_{i\tau_3\sigma} a_{i\sigma}^\dagger a_{i+\tau_3\sigma}], \\
H_3 &= t_1^{Ni} [\sum_{i\tau_1\sigma} b_{i\sigma}^\dagger b_{i+\tau_1\sigma}] + t_2^{Ni} [\sum_{i\tau_2\sigma} b_{i\sigma}^\dagger b_{i+\tau_2\sigma}] \\
&\quad + t_3^{Ni} [\sum_{i\tau_3\sigma} b_{i\sigma}^\dagger b_{i+\tau_3\sigma}], \\
H_4 &= U \sum_{\mathbf{i}} n_{b\mathbf{i}\uparrow} n_{b\mathbf{i}\downarrow} + \mu \sum_{\mathbf{i}\sigma} [(1 + \Delta/\mu) n_{a\mathbf{i}\sigma} + n_{b\mathbf{i}\sigma}] \quad (1)
\end{aligned}$$

Here,  $a_{i\sigma}$  ( $a_{i\sigma}^\dagger$ ) annihilates (creates) electrons at site  $\mathbf{R}_i$  with spin  $\sigma$  ( $\sigma=\uparrow, \downarrow$ ) on sublattice A,  $b_{i\sigma}$  ( $b_{i\sigma}^\dagger$ ) annihilates (creates) electrons at site  $\mathbf{R}_i$  with spin  $\sigma$  ( $\sigma=\uparrow, \downarrow$ ) on sublattice B,  $n_{a\mathbf{i}\sigma} = a_{i\sigma}^\dagger a_{i\sigma}$ ,  $n_{b\mathbf{i}\sigma} = b_{i\sigma}^\dagger b_{i\sigma}$ ,  $\eta = (\pm 3\hat{x}, \pm 3\hat{y})$ ,  $\tau_1 = (\pm 2\hat{x}, 0)$  and  $(0, \pm 2\hat{y})$ , and  $\tau_2 = (\pm 2\hat{x}, \pm 2\hat{y})$ , and  $\tau_3 = (\pm 4\hat{x}, 0)$  and  $(0, \pm 4\hat{y})$ . Our first-

principles calculations are basically consistent with the data in Refs.[10, 36, 37]. For more details about our Wannier downfolding of NdNiO<sub>2</sub>, please see Table II in the supplementary materials. For simplicity and clarity, we mainly take the parameters from Refs.[10, 36, 37] and list the hopping parameters of NdNiO<sub>2</sub> in Table I at  $k_z=0$ ,  $\pi/2$  and  $\pi$ . From the analysis of the first-principles calculations[10, 36, 37, 41, 42],  $\Delta=\Delta_1-\Delta_2$  represents the on-site energy difference between the Nd 5d orbital and the Ni 3d orbital. In the following calculations, we mainly discuss the cases of  $k_z=0$  and  $k_z = \pi$ .

Our simulations are mainly performed on the lattice shown in Fig. 1(a) of  $L=8$  (the total number of lattice sites is  $N_s=2 \times L^2=128$ ) by using the determinant quantum Monte Carlo (DQMC) method at finite temperature with periodic boundary conditions. The basic strategy of the DQMC method is to express the partition function as high-dimensional integrals on a set of random auxiliary fields. Then, the Monte Carlo techniques complete the integral. In the simulations, we use 3000 sweeps to equilibrate the system and an additional 10000 sweeps to generate measurements. These measurements were split into 10 bins and provided the basis of coarse-grain averages. The errors were calculated based on the standard deviation from the average. For more technical details, please see Refs.[43–45].

As magnetic excitation possibly plays a significant role in the superconductivity mechanism of electronically correlated systems, we investigate the spin susceptibility in the z direction at zero frequency,

$$\chi(q) = \int_0^\beta d\tau \sum_{d,d'=a,b} \sum_{\mathbf{i},\mathbf{j}} e^{iq \cdot (\mathbf{i}_d - \mathbf{j}_{d'})} \langle \mathbf{m}_{\mathbf{i}_d}(\tau) \cdot \mathbf{m}_{\mathbf{j}_{d'}}(0) \rangle, \quad (2)$$

where  $m_{i_a}(\tau) = e^{H\tau} m_{i_a}(0) e^{-H\tau}$  with  $m_{i_a} = a_{i\uparrow}^\dagger a_{i\uparrow} - a_{i\downarrow}^\dagger a_{i\downarrow}$  and  $m_{i_b} = b_{i\uparrow}^\dagger b_{i\uparrow} - b_{i\downarrow}^\dagger b_{i\downarrow}$ . To study the superconducting property of nickelate-based superconductors, we calculated the pairing susceptibility,

$$P_\alpha = \frac{1}{N_s} \sum_{\mathbf{i},\mathbf{j}} \int_0^\beta d\tau \langle \Delta_\alpha^\dagger(\mathbf{i}, \tau) \Delta_\alpha(\mathbf{j}, 0) \rangle, \quad (3)$$

where  $\alpha$  denotes the pairing symmetry. Due to the constraint of different on-site Hubbard interaction in two sublattices, pairing between the same sublattices is favoured, and the corresponding order parameter  $\Delta_\alpha^\dagger(\mathbf{i})$  is written as

$$\Delta_\alpha^\dagger(\mathbf{i}) = \sum_l f_\alpha^\dagger(\delta_l) (a_{i\uparrow}^\dagger b_{i+\delta_l\downarrow} - a_{i\downarrow}^\dagger b_{i+\delta_l\uparrow})^\dagger,$$

where  $f_\alpha(\delta_l)$  stands for the form factor of pairing function. The vectors  $\delta_l$  ( $l=1,2,3,4$ ) represent the nearest intersublattice connections, where  $\delta$  is  $(\pm\hat{x}, \pm\hat{y})$ , or the

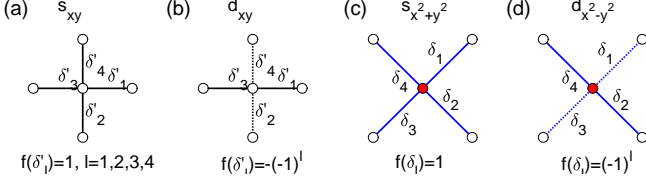


FIG. 2. (Color online) Phase of the  $s_{xy}$ ,  $d_{xy}$ ,  $s_{x^2+y^2}$  and  $d_{x^2-y^2}$ .

nearest intrasublattice connections where  $\delta'$  is  $(\pm 2\hat{x}, 0)$  and  $(0, \pm 2\hat{y})$ .

We referenced four kinds of pairing forms from the iron-square lattice[45], which are pictured in Fig. 2. These singlet  $s$ -wave and  $d$ -wave pairings have the form factor

$$\begin{aligned}
 s_{xy}\text{-wave} &: f_{s_{xy}}(\delta'_l) = 1, \quad l = 1, 2, 3, 4, \\
 d_{xy}\text{-wave} &: f_{d_{xy}}(\delta'_l) = 1(\delta'_l = (\pm 2\hat{x}, 0)) \\
 &\quad \text{and} \quad f_{d_{xy}}(\delta'_l) = -1(\delta'_l = (0, \pm 2\hat{y})), \\
 s_{x^2+y^2}\text{-wave} &: f_{s_{x^2+y^2}}(\delta'_l) = 1, \quad l = 1, 2, 3, 4, \\
 d_{x^2-y^2}\text{-wave} &: f_{d_{x^2-y^2}}(\delta'_l) = 1(\delta'_l = \pm(-\hat{x}, \hat{y})) \\
 &\quad \text{and} \quad f_{d_{x^2-y^2}}(\delta'_l) = -1(\delta'_l = \pm(\hat{x}, \hat{y})). \quad (4)
 \end{aligned}$$

*Results and discussion* To study the magnetic correlations, we calculated the spin susceptibility  $\chi(\mathbf{q})$  in Fig. 3 at different  $U$  and fillings  $\langle n \rangle$  at temperature  $T=1/6$ . In Fig. 3(a) and Fig. 3(b), one can notice that there is a smooth peak at  $(\pi, \pi)$ , which indicates the existence of AFM correlation at  $k_z = 0$ . In Fig. 3(a), we can see that the AFM correlation is enhanced as  $U$  increases, which indicates that such an AFM correlation is driven by strong electron-electron correlation. Fig. 3(b) shows that the peak is almost identical at different fillings, which indicates that the AFM correlation is nearly unchanged when the system is doped away from half filling. However, from Fig. 3(c) and Fig. 3(d) at  $k_z = \pi$ , we can see a small transition from FM to AFM as the filling decreases from 1.0. Recently, resonant inelastic X-ray scattering experiments revealed an AFM exchange interaction[46]. Our results here might provide evidence for the AFM exchange couplings observed in nickelate-based superconductors.

In Fig. 4(a), we show the temperature dependence of the pairing susceptibilities for different pairing symmetries at half filling with  $U=1.122$  at  $k_z = 0$ . We can clearly observe that the pairing susceptibilities for various pairing symmetries increase with decreasing temperature. Most strikingly,  $d_{xy}$  increases much faster than any other pairings symmetry as the temperature is lowered. This indicates that the  $d_{xy}$  pairing symmetry is dominant over the other pairing symmetry at half filling. Our further results also illustrate that the  $d_{xy}$  pairing symmetry is robust at different fillings and  $U$ .

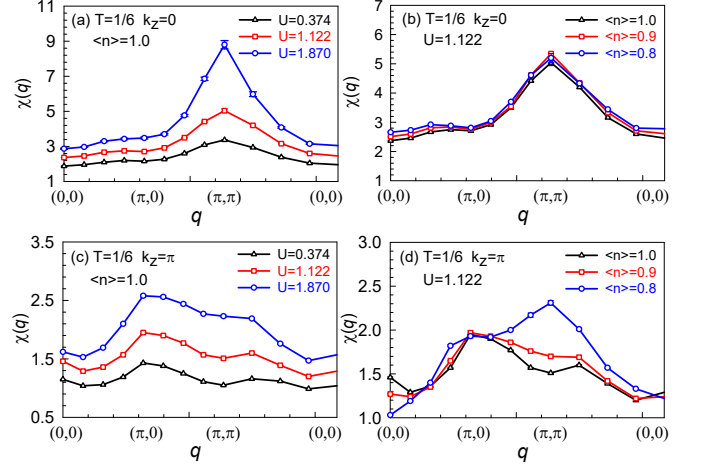


FIG. 3. (Colour online) (a) Magnetic susceptibility  $\chi(q)$  versus momentum  $q$  for different  $U$  at  $\langle n \rangle = 1.0$  and  $k_z = 0$  on a  $2 \times 8^2$  lattice. (b) Magnetic susceptibility  $\chi(q)$  versus momentum  $q$  for different fillings at  $U = 1.122$  and  $k_z = 0$  on a  $2 \times 8^2$  lattice. (c) Magnetic susceptibility  $\chi(q)$  versus momentum  $q$  for different  $U$  at  $\langle n \rangle = 1.0$  and  $k_z = \pi$  on a  $2 \times 8^2$  lattice. (d) Magnetic susceptibility  $\chi(q)$  versus momentum  $q$  for different fillings at  $U = 1.122$  and  $k_z = \pi$  on a  $2 \times 8^2$  lattice.

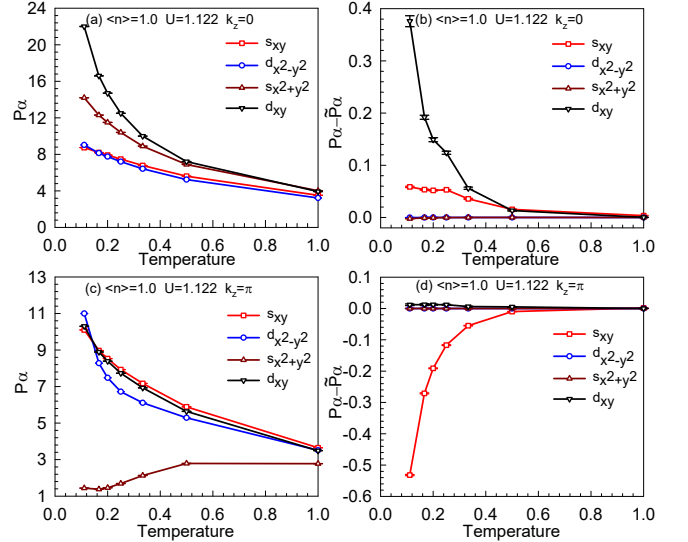


FIG. 4. (Color online) (a) Pairing susceptibility  $P_\alpha$  as a function of temperature for different pairing symmetries at  $\langle n \rangle = 1.0$ ,  $U = 1.122$  and  $k_z = 0$  on a  $2 \times 8^2$  lattice. (b) The effective pairing interaction  $P_\alpha - \tilde{P}_\alpha$  as a function of temperature for different pairing symmetries at  $\langle n \rangle = 1.0$ ,  $U = 1.122$ , and  $k_z = 0$  on a  $2 \times 8^2$  lattice. (c) Pairing susceptibility  $P_\alpha$  as a function of temperature for different pairing symmetries at  $\langle n \rangle = 1.0$ ,  $U = 1.122$  and  $k_z = \pi$  on a  $2 \times 8^2$  lattice. (d) The effective pairing interaction  $P_\alpha - \tilde{P}_\alpha$  as a function of temperature for different pairing symmetries at  $\langle n \rangle = 1.0$ ,  $U = 1.122$ , and  $k_z = \pi$  on a  $2 \times 8^2$  lattice.

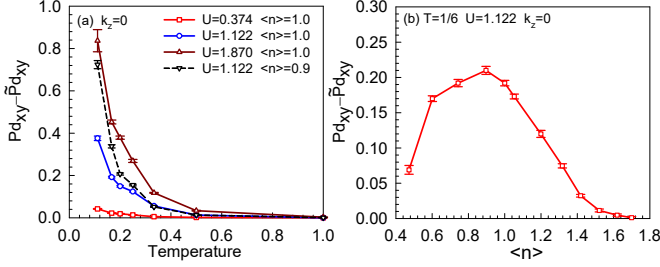


FIG. 5. (Colour online) (a) The effective pairing interaction  $P_{d_{xy}} - \tilde{P}_{d_{xy}}$  as a function of temperature for different  $U$  at  $\langle n \rangle = 1.0$  and  $k_z = 0$  on a  $2 \times 8^2$  lattice. (b) The effective pairing interaction  $P_{d_{xy}} - \tilde{P}_{d_{xy}}$  as a function of fillings at  $T = 1/6$ ,  $U = 1.122$  and  $k_z = 0$  on a  $2 \times 8^2$  lattice.

The effective pairing interaction is a direct probe for the superconductivity. To extract the effective pairing interaction, the uncorrelated single-particle contribution  $\tilde{P}_\alpha(\mathbf{i}, \mathbf{j})$  is calculated, which is achieved by replacing  $\langle a_{i\downarrow}^\dagger b_{j\uparrow} a_{i+\delta_{i\downarrow}}^\dagger b_{j+\delta_{i\downarrow}} \rangle$  in Eq. 3 with  $\langle a_{i\downarrow}^\dagger b_{j\uparrow} \rangle \langle a_{i+\delta_{i\downarrow}}^\dagger b_{j+\delta_{i\downarrow}} \rangle$ , and then we get the effective pairing interaction  $P_\alpha - \tilde{P}_\alpha$ . In Fig. 4(b), it is obvious that  $P_\alpha - \tilde{P}_\alpha$  presents a very similar temperature dependence to that of  $P_\alpha$ . Moreover, the effective pairing interaction for  $d_{xy}$  pairing is always positive and increases much faster than any other pairing symmetry at low temperatures. Such a temperature dependence shows that there indeed exists attraction for the  $d_{xy}$  pairing at  $k_z = 0$ . From Fig. 4(c) and Fig. 4(d), we cannot find that pairing symmetry always increases at low temperatures and that the effective pairing interaction for all pairing symmetries is very small. Therefore, as the hopping parameter  $t_i^N d$  changes, the investigated effective pairing interaction with the four pairing symmetries might disappear. In the following, we mainly discuss the hopping parameter for  $k_z = 0$ .

Fig. 5(a) shows the effective pairing interaction as a function of temperature for the  $d_{xy}$  wave at different  $U$ . We can see that the effective pairing interaction of the  $d_{xy}$  wave is enhanced with increasing  $U$ . For  $U=0.374$ , the effective pairing interaction  $P_{d_{xy}} - \tilde{P}_{d_{xy}}$  is very small even in the low-temperature region, which may be due to the small AFM structure of the system in Fig. 3(a). For  $U=1.122$  and  $U=1.870$ , remarkably, the effective pairing interaction  $P_{d_{xy}} - \tilde{P}_{d_{xy}}$  tends to diverge at low temperatures, and with increasing  $U$ , this divergence tends to be promoted. This indicates that the  $d_{xy}$  pairing superconductivity should be driven by a strong electron-electron correlation.

In Fig. 5(b), we studied the filling dependence of the effective pairing interaction  $P_{d_{xy}} - \tilde{P}_{d_{xy}}$  at  $T = 1/6$ ,  $U = 1.122$  and  $k_z = 0$ . Fig. 5 (b) indicates that the effective pairing interaction  $P_{d_{xy}} - \tilde{P}_{d_{xy}}$  is the largest around filling 0.9. As shown in Fig. 3 and Fig. 5 show that the increase in the peak at  $(\pi, \pi)$  of spin

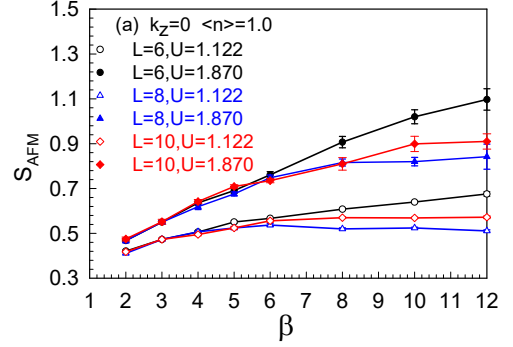


FIG. 6. (Colour online) The AFM spin structure factor  $S_{AFM}$  depends on  $\beta = 1/T$  with different interaction strengths and lattice sizes at  $\langle n \rangle = 1.0$  and  $k_z = 0$ .

susceptibility is correlated with the promotion of the pairing susceptibility. This directly confirms that the  $(\pi, \pi)$  AFM fluctuations enhance the  $d_{xy}$  pairing.

From the above studies, we know that the system exhibits local antiferromagnetism. To further explore whether there is a long-range AFM order, we also calculate the AFM spin structure factor,

$$S_{AFM} = \frac{1}{N_s} \langle [\sum_r (-1)^r \hat{S}_{br}^z]^2 \rangle, \quad (5)$$

Here,  $\hat{S}_{br}^z$  is the  $z$  component spin operator on the B sublattice. When  $\lim_{N_s \rightarrow \infty} (S_{AFM}/N_s) > 0$ , it indicates the onset of long-range AFM order. In Fig. 6, we investigate the AFM spin structure factor behaviours versus the inverse temperature  $\beta$  for different interaction strengths  $U$  and lattice sizes  $L$ . We can see that  $S_{AFM}$  decreases as the lattice size increases at low temperatures, which indicates no long-range AFM order at  $U < 1.870$ .

In summary, within an effective two-band model for nickelate-based superconductors, we study the spin correlation and the superconducting pairing interaction by using the unbiased numerical techniques of DQMC. We identify that the  $d_{xy}$  wave pairing channel is dominant in nickelate-based superconductors, which is consistent with the recent london penetration depth experiment[47]. Both the  $(\pi, \pi)$  AFM and the pairing susceptibility of the  $d_{xy}$  symmetry is enhanced with increasing electron-electron correlation, especially in the low-temperature region. Moreover, As the electronic filling decreases from half filling, the pairing susceptibility of  $d_{xy}$  symmetry is also enhanced around  $\langle n \rangle = 0.9$ . Our results also indicate that the system may not exhibit long-range AFM, which is also not observed experimentally[46]. Our work shares exact numerical results to understand the superconducting mechanism of nickelate-based materials.

*Acknowledgements* — We thank Huijia Dai and Jingyao Meng for useful discussions. This work was supported

by NSFC (No. 11974049). The numerical simulations in this work were performed at the HSCC of Beijing Normal University and Tianhe in Beijing Computational Science Research Center.

### Supplemental Material

In consideration of the two-band model in our Hamiltonian, we chose orbital sets of  $Ni_{3d_{x^2-y^2}}$  and  $Nd/La_{5d_{z^2}}$  in Wannier downfolding calculations as implemented in Wannier90[48], which can reproduce the band structure near the Fermi level accurately. The calculated hopping parameters for two-orbital Wannierization are listed in Table II.

Hopping parameters for the tight binding model				
			$NdNiO_2$	$LaNiO_2$
i	j	k	$t_{[i,j,k]}^{Ni}$	
0	0	0	5.953385	8.524621
1	0	0	-0.377362	-0.380994
1	1	0	0.094731	0.095830
2	0	0	-0.049510	-0.049076
0	0	1	-0.027912	-0.032524
1	0	1	-0.001615	0.000423
1	1	1	0.008920	0.009345
0	0	2	0.001415	0.000151
0	0	3	-0.000053	0.001201
			$t_{[i,j,k]}^{Nd/La}$	
0	0	0	7.743987	9.109156
1	0	0	-0.470838	-0.068788
1	1	0	-0.021513	-0.087446
2	0	0	0.051356	0.021989
0	0	1	-0.293301	-0.048961
1	0	1	0.015698	-0.196251
1	1	1	0.004019	-0.005498
0	0	2	0.027121	-0.099677
0	0	3	0.006169	-0.003715
			$t_{[i,j,k]}^{Nd/La-Ni}$	
0	0	0	0.000151	-0.011252
1	0	0	-0.000239	0.009664
1	1	0	-0.000037	0.003106
2	0	0	-0.001777	0.001579
0	0	1	-0.000157	-0.006010
1	0	1	-0.007317	0.008403
1	1	1	0.000070	0.006332
0	0	2	0.000102	-0.004345
0	0	3	-0.000040	-0.001681

TABLE II. On-site energy and hopping parameters for two-orbital wannierization for  $NdNiO_2$  and  $LaNiO_2$ .

- [1] J. Bardeen, L. N. Cooper, and J. R. Schrieffer, *Phys. Rev.* **108**, 1175 (1957).
- [2] J. G. Bednorz and K. A. Müller, *Zeitschrift für Physik B Condensed Matter* **64**, 189 (1986).
- [3] P. W. Anderson, *Science* **235**, 1196 (1987).
- [4] J. G. Bednorz and K. A. Müller, *Rev. Mod. Phys.* **60**, 585 (1988).
- [5] P. W. Anderson, P. A. Lee, M. Randeria, T. M. Rice, N. Trivedi, and F. C. Zhang, *Journal of Physics: Condensed Matter* **16**, R755 (2004).
- [6] P. A. Lee, N. Nagaosa, and X.-G. Wen, *Rev. Mod. Phys.* **78**, 17 (2006).
- [7] D. J. Scalapino, *Rev. Mod. Phys.* **84**, 1383 (2012).
- [8] D. Li, K. Lee, B. Y. Wang, M. Osada, S. Crossley, H. R. Lee, Y. Cui, Y. Hikita, and H. Y. Hwang, *Nature* **572**, 624 (2019).
- [9] G. A. Sawatzky, *Nature* **572**, 592 (2019).
- [10] M. Hepting, D. Li, C. J. Jia, H. Lu, E. Paris, Y. Tseng, X. Feng, M. Osada, E. Been, Y. Hikita, Y.-D. Chuang, Z. Hussain, K. J. Zhou, A. Nag, M. Garcia-Fernandez, M. Rossi, H. Y. Huang, D. J. Huang, Z. X. Shen, T. Schmitt, H. Y. Hwang, B. Moritz, J. Zaanen, T. P. Devereaux, and W. S. Lee, *Nature Materials* **19**, 381 (2020).
- [11] M.-Y. Choi, K.-W. Lee, and W. E. Pickett, *Phys. Rev. B* **101**, 020503 (2020).
- [12] C. Peng, H.-C. Jiang, B. Moritz, T. P. Devereaux, and C. Jia, (2021), [arXiv:2110.07593](https://arxiv.org/abs/2110.07593).
- [13] L. Si, W. Xiao, J. Kaufmann, J. M. Tomczak, Y. Lu, Z. Zhong, and K. Held, *Phys. Rev. Lett.* **124**, 166402 (2020).
- [14] S. Ryee, H. Yoon, T. J. Kim, M. Y. Jeong, and M. J. Han, *Phys. Rev. B* **101**, 064513 (2020).
- [15] S. Zeng, C. S. Tang, X. Yin, C. Li, M. Li, Z. Huang, J. Hu, W. Liu, G. J. Omar, H. Jani, Z. S. Lim, K. Han, D. Wan, P. Yang, S. J. Pennycook, A. T. S. Wee, and A. Ariando, *Phys. Rev. Lett.* **125**, 147003 (2020).
- [16] J. Krishna, H. LaBollita, A. O. Fumega, V. Pardo, and A. S. Botana, *Phys. Rev. B* **102**, 224506 (2020).
- [17] M. Osada, B. Y. Wang, K. Lee, D. Li, and H. Y. Hwang, *Phys. Rev. Materials* **4**, 121801 (2020).
- [18] Y. Cui, C. Li, Q. Li, X. Zhu, Z. Hu, Y. feng Yang, J. Zhang, R. Yu, H.-H. Wen, and W. Yu, *Chinese Physics Letters* **38**, 067401 (2021).
- [19] P. Jiang, L. Si, Z. Liao, and Z. Zhong, *Phys. Rev. B* **100**, 201106 (2019).
- [20] B.-X. Wang, H. Zheng, E. Kriviyakina, O. Chmaissem, P. P. Lopes, J. W. Lynn, L. C. Gallington, Y. Ren, S. Rosenkranz, J. F. Mitchell, and D. Phelan, *Phys. Rev. Materials* **4**, 084409 (2020).
- [21] D. Li, B. Y. Wang, K. Lee, S. P. Harvey, M. Osada, B. H. Goodge, L. F. Kourkoutis, and H. Y. Hwang, *Phys. Rev. Lett.* **125**, 027001 (2020).
- [22] K. Lee, B. H. Goodge, D. F. Li, M. Osada, B. Y. Wang, Y. Cui, L. F. Kourkoutis, and H. Y. Hwang, *APL MATERIALS* **8** (APR 1), 10.1063/5.0005103.
- [23] M. Osada, B. Y. Wang, B. H. Goodge, S. P. Harvey, K. H. Lee, D. F. Li, L. F. Kourkoutis, and H. Y. Hwang, *Adv.Mater.* **33**, 2104083 (2021).
- [24] S. Zeng, C. Li, L. E. Chow, Y. Cao, Z. Zhang, C. S. Tang, X. Yin, Z. S. Lim, J. Hu, P. Yang, and A. Ariando, *Science Advances* **8**, eabl9927 (2022).
- [25] Q. Gu, Y. Li, S. Wan, H. Li, W. Guo, H. Yang, Q. Li, X. Zhu, X. Pan, Y. Nie, and H.-H. Wen, *Nature*

\* [txma@bnu.edu.cn](mailto:txma@bnu.edu.cn)

- Communications* **11**, 6027 (2020).
- [26] M. Zhang, Y. Zhang, H. Guo, and F. Yang, *Chinese Physics B* **30**, 108204 (2021).
- [27] Y.-H. Zhang and A. Vishwanath, *Phys. Rev. Research* **2**, 023112 (2020).
- [28] P. Adhikary, S. Bandyopadhyay, T. Das, I. Dasgupta, and T. Saha-Dasgupta, *Phys. Rev. B* **102**, 100501 (2020).
- [29] X. Wu, D. Di Sante, T. Schwemmer, W. Hanke, H. Y. Hwang, S. Raghu, and R. Thomale, *Phys. Rev. B* **101**, 060504 (2020).
- [30] G.-M. Zhang, Y.-f. Yang, and F.-C. Zhang, *Phys. Rev. B* **101**, 020501 (2020).
- [31] C. Lu, L.-H. Hu, Y. Wang, F. Yang, and C. Wu, *Phys. Rev. B* **105**, 054516 (2022).
- [32] H. Sakakibara, H. Usui, K. Suzuki, T. Kotani, H. Aoki, and K. Kuroki, *Phys. Rev. Lett.* **125**, 077003 (2020).
- [33] Z. Wang, G.-M. Zhang, Y.-f. Yang, and F.-C. Zhang, *Phys. Rev. B* **102**, 220501 (2020).
- [34] V. I. Anisimov, D. Bukhvalov, and T. M. Rice, *Phys. Rev. B* **59**, 7901 (1999).
- [35] K.-W. Lee and W. E. Pickett, *Phys. Rev. B* **70**, 165109 (2004).
- [36] A. S. Botana and M. R. Norman, *Phys. Rev. X* **10**, 011024 (2020).
- [37] E. Been, W.-S. Lee, H. Y. Hwang, Y. Cui, J. Zaanen, T. Devereaux, B. Moritz, and C. Jia, *Phys. Rev. X* **11**, 011050 (2021).
- [38] M. Jiang, M. Berciu, and G. A. Sawatzky, *Phys. Rev. Lett.* **124**, 207004 (2020).
- [39] Y. Nomura, M. Hirayama, T. Tadano, Y. Yoshimoto, K. Nakamura, and R. Arita, *Phys. Rev. B* **100**, 205138 (2019).
- [40] L.-H. Hu and C. Wu, *Phys. Rev. Research* **1**, 032046 (2019).
- [41] J. Karp, A. S. Botana, M. R. Norman, H. Park, M. Zingl, and A. Millis, *Phys. Rev. X* **10**, 021061 (2020).
- [42] F. Lechermann, *Phys. Rev. X* **10**, 041002 (2020).
- [43] R. Blankenbecler, D. J. Scalapino, and R. L. Sugar, *Phys. Rev. D* **24**, 2278 (1981).
- [44] T. Ma, F. Hu, Z. Huang, and H.-Q. Lin, *Applied Physics Letters* **97**, 112504 (2010).
- [45] T. Ma, H.-Q. Lin, and J. Hu, *Phys. Rev. Lett.* **110**, 107002 (2013).
- [46] H. Lu, M. Rossi, A. Nag, M. Osada, D. F. Li, K. Lee, B. Y. Wang, M. Garcia-Fernandez, S. Agrestini, Z. X. Shen, E. M. Been, B. Moritz, T. P. Devereaux, J. Zaanen, H. Y. Hwang, K.-J. Zhou, and W. S. Lee, *Science* **373**, 213 (2021).
- [47] S. P. Harvey, B. Y. Wang, J. Fowlie, M. Osada, K. Lee, Y. Lee, D. Li, and H. Y. Hwang, (2022), [arXiv:2201.12971](https://arxiv.org/abs/2201.12971).
- [48] A. A. Mostofi, J. R. Yates, Y.-S. Lee, I. Souza, D. Vanderbilt, and N. Marzari, *Computer Physics Communications* **178**, 685 (2008).